Entropy-Induced Frozen Morphology in Unstable Polymer Blends

Mahesh A. Kotnis and M. Muthukumar*

Polymer Science and Engineering Department, University of Massachusetts at Amherst, Amherst, Massachusetts 01003

Received October 9, 1991

ABSTRACT: We report the arrest of spinodal decomposition for thermodynamically unstable off-critical polymer blends. A coarsening mechanism based on the entropic barrier created for the transport of long chains across sharp interfaces between the phase-separated domains can explain this novel feature characteristic of polymer blends. The relative contributions of the enthalpic and entropic parts of the free energy of an inhomogeneous polymer mixture to the kinetics of phase separation are computed. For polymers the entropic contribution dominates and leads to the emergence of a transnodal regime.

Introduction

The study of phase separation in polymer blends has been of considerable technological importance in order to develop new materials to achieve specific end properties. The chainlike nature of macromolecules results in the small entropy of mixing, and polymer systems are usually thermodynamically immiscible. It is well-known that the morphological and interfacial properties of these systems play an important role in most of their practical applications. The phenomenon of phase separation in polymer mixtures has recently attracted many experimental and theoretical investigations, due to the fact[1-4] that such polymer mixtures belong to the same universality class as the small-molecule systems such as binary alloys and fluid mixtures and due to the ease with which the critical fluctuations can be probed for widely varying experimental parameters. It is well-known[5] in small-molecule systems that the spinodal decomposition (SD) type of phase separation occurs in the unstable region where fluctuations grow without any barrier, while the nucleation and growth (NG) type of phase separation occurs in the metastable region because of the existence of the barrier of nucleation. The objective in the present study of phase separation of polymer mixtures is to discover possible unique characteristics originating from the presence of long-chain molecules.

Consider an A–B polymer mixture, with chain lengths $N_A = N = N_B$ and Kuhn lengths $a_A = a = a_B$, undergoing phase separation by the SD mechanism. Depending upon the growth rates of the wavelength and the amplitude of concentration fluctuations, the SD process is characterized by three distinct time scales: early, intermediate, and late stages. In the early stage of SD the structure formed from the thermodynamically unstable state is percolated irrespective of the initial composition of the mixture and is characteristic of the spinodal process. However, as SD proceeds during the intermediate stage, when the domain size increases and the compositions get closer to their equilibrium values, it is possible to realize two scenarios as in parts a and b of Figure 1 depending upon the relative volume fractions of the two phases. Figure 1a represents a situation where the volume fraction of the minority phase, say the A-rich phase, is less than the percolation threshold so that the domains of the A-rich phase are dispersed in the matrix of the B-rich phase. Figure 1b corresponds to a situation of comparable volume fractions of the two phases so that the two phases are percolating at the intermediate stage of SD.

Now consider the further evolution of the patterns shown in Figure 1 via the familiar Lifshitz–Slyozov type evaporation–condensation mechanism. The growth of the A-rich domains occurs by the transport of A-type polymer chains from one location to another. We distinguish two mechanisms of this transport. In the first, an A-type polymer chain needs to be pulled out of an A-rich domain across the interface into the B-rich phase followed by the diffusion and further condensation into another A-rich domain. In the second mechanism polymer chains diffuse parallel to the interface and the structure undergoes continuous reorganization of interfaces so as to reduce the overall interfacial free energy. In this case the coarsening of domains occurs by the interfacial dynamics. The interfaces in the intermediate and late stages of SD are sharp enough to cause a significant loss of conformational entropy of polymer chains.[6-8] Therefore, there exists an entropic barrier, proportional to the chain length N, for chain transport across the interface. Consequently the characteristic time needed for the chain transport in the first mechanism is porportional to $N^3 \exp(Nf)$ where N^3 is the reptation[9] time and the exponential term is the amplitude reflecting the time needed to cross the entropic barrier at the interface. The factor f is a function of the concentration difference between the A-rich and the A-poor domains. This is to be contrasted with the second mechanism where the time scale is on the order of the reptation time N^3. Since N for polymer blends is very large, we expect the first mechanism to be effectively suppressed irrespective of the intermediate patterns in Figure 1. The second mechanism of growth by the interfacial dynamics does not lead to any domain growth in the scenario of Figure 1a while ripening is allowed in Figure 1b. Therefore, when the composition is such that the minority phase is not percolating, we expect the coarsening to be effectively stopped, while the coarsening continues if the resulting phases are percolating. Thus a new region is expected for polymer mixtures with a frozen morphology inside the unstable region, and it is associated with the transition from percolated to dispersed clusters and the dominance of the entropic contribution to the

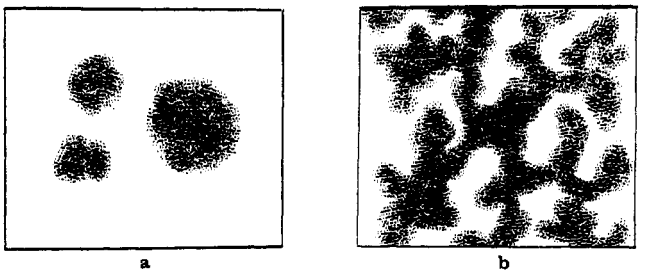

Figure 1. (a) Minority phase dispersed in the majority phase. (b) Two phases after percolation.

0024-9297/92/2225-1716$03.00/0

interfacial free energy. We show below for polymer mixtures that there indeed exists a region within the SD regime where domain growth is arrested.

Dynamics of Spinodal Decomposition in Polymer Mixtures

The theoretical understanding of the spinodal decomposition process in small-molecule systems is based on the Cahn–Hilliard–Cook formulation.[10] In this formulation the free energy of the inhomogeneous mixture (i.e., having regions of nonuniform composition) of volume V is described by the coarse-grained free energy functional $F(\phi(r))$ given by

$$F(\phi(r)) = \int d^3r\, [f(\phi(r)) + \kappa|\nabla\phi(r)|^2] \qquad (1)$$

where $f(\phi)$ is the free energy density of a uniform composition ϕ and $\kappa|\nabla\phi|^2$ is the positive contribution to the free energy density from the local composition gradients. For small molecules the prefactor of the square gradient term κ is given by $\kappa = \chi\lambda^2$ where χ is the interaction parameter between the two species in the mixture and λ is the effective interaction length between the molecules. Analytical studies of this model have been reasonably successful in describing the early time behavior of the phase-separation process, but due to their linearized nature they are not useful in the later stages.[5] It is necessary to perform a numerical study of the continuity equation to explore the nonlinear behavior of the phase-separation kinetics at late time scales. Numerical studies and Monte Carlo simulations in critical and off-critical mixtures of small-molecule systems have suggested that the characteristic size of the domains shows a Lifshitz–Slyozov type growth law independent of the final quench temperature and these systems obey universal scaling laws.[11-16] There have been various theories to predict the growth laws for the coarsening of the domains in the off-critical[17] as well as critical[18] mixtures, but it still remains a challenging problem in nonequilibrium statistical mechanics.

The earliest attempts to study the kinetics of spinodal decomposition in polymer blends were due to Nishi et al.[19] and Mcmaster.[20] In both the cases the experimental data were analyzed using Debye's free energy functional[21] which was employed to describe the free energy of inhomogeneous polymer mixtures. This (Debye) free energy is similar to the Cahn–Hilliard functional in eq 1 with $f(\phi)$ equal to the Flory–Huggins (F–H) free energy and with λ on the order of the radius of gyration of the polymer chain. The prefactor of the square gradient term in this free energy functional is a constant term (independent of local composition) and has its origin in the enthalpic contribution to the interfacial free energy. The idea that the chain connectivity of polymer molecules significantly affects the nature of polymer–polymer interfaces was pioneered by Helfand[7] in the early 1970s. Helfand and co-workers constructed a self-consistent-field theory of polymer–polymer interfaces by solving the segmental diffusion equation across the interface. They showed that the interfacial tension γ and the interfacial thickness D for a symmetric polymer blend are given by

$$\gamma = (kT/a^2)(\chi/6)^{1/2} \text{ and } D = 2a/(6\chi)^{1/2} \qquad (2)$$

where a is the Kuhn length and χ is the F–H interaction parameter. Thus the interfacial thickness D can be on the order of a few Kuhn lengths, much smaller than the actual size of the polymer chain. Later de Gennes[22] proposed a free energy functional to describe the free energy of inhomogeneous polymer blends where he argued that the chain connectivity of polymer molecules manifests itself in the form of an entropic contribution to the square gradient term in addition to the usual enthalpic contribution. He evaluated this entropic contribution within the framework of the random-phase approximation (RPA). He also argued that since the thickness of the interface is on the order of a few Kuhn lengths and since the interaction parameter for most of the polymer–polymer systems is typically very small (on the order of 10^{-2} or so), the entropic contribution will override the enthalpic contribution. Widom and Szleifer[8] derived the prefactor of the square gradient term for inhomogeneous polymer solutions by modifying Helfand's original scheme of self-consistent-field calculations. They were able to show that the prefactor obtained from the RPA arguments indeed stems from the loss of conformational entropy of polymer chains at the interface, and this in turn results in the entropic contribution to the interfacial free energy. Tang and Freed[23] have rederived de Gennes free energy functional from the density functional theory of inhomogeneous polymer blends. Using de Gennes free energy functional, analytical studies of SD in polymer blends were carried out in the linear regime.[22,24] Because of the mathematical complexity of incorporating nonlinear effects, it is very difficult to do analytical work describing the intermediate and late stages of the SD process. In the absence of analytical studies, numerical studies and Monte Carlo simulations have been found extremely useful to understand and predict the late time behavior of the SD process in small-molecule systems.[11-16] Along the same lines similar techniques have been recently employed to gain insight into the late stage dynamics of SD in polymer mixtures. Monte Carlo simulations of SD in a ternary system consisting of two polymers and a solvent have been reported by Sariban and Binder.[25] Chakrabarti et al.[26] have reported the numerical study of SD in a symmetric polymer blend in three dimensions. They have employed the Flory–Huggins–de Gennes (FHD) free energy functional[22] to describe the free energy of the inhomogeneous polymer mixture. In their study the Onsager coefficient was taken as constant and only the dynamics of critical mixtures was explored. In this paper we have included the composition dependence of the Onsager coefficient and have investigated the dynamics of critical as well as off-critical mixtures.

Consider a volume element of a phase-separating polymer blend for which the following set of phenomenological equations can be written.[22]

$$\frac{d\phi(r,t)}{dt} = -\nabla J_A + \eta(r,t) \qquad (3a)$$

$$J_A = \frac{\Lambda(\phi)}{k_B T}\nabla\left(\frac{\delta F(\phi(r))}{\delta\phi}\right) \qquad (3b)$$

Here the order parameter $\phi(r,t)$ is the volume fraction of component A at position r and time t, and J_A is the local current of component A. $\delta F(\phi(r))/\delta\phi$ is the functional derivative of a coarse-grained free energy functional $F(\phi(r))$, and $\Lambda(\phi)$ is the Onsager coefficient. k_B is the Boltzmann constant, T is the absolute temperature, and $\eta(r,t)$ is the thermal noise.

The Onsager coefficient is in general a function of ϕ and should be consistent with the free energy $F(\phi)(r))$. In the Cahn–Hilliard–Cook formulation it was taken as a constant which simplifies eq 3 as

$$\frac{d\phi(r,t)}{dt} = M\nabla^2\frac{\delta F(\phi(r))}{\delta\phi} + \eta(r,t) \qquad (4)$$

where $M = \Lambda/k_B T$ and $\eta(r,t)$ satisfies the fluctuation–

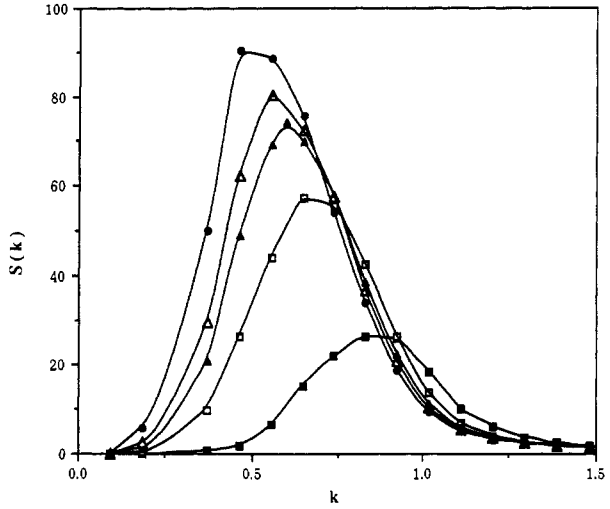

Figure 2. Spherically averaged structure factor $S(k,\tau)$ vs k for different values of τ calculated for the critical mixture ($\phi_0 = 0.5$) quenched to 49 °C. The symbols are as follows: (■) $\tau = 22$ (□) $\tau = 112$, (▲) $\tau = 225$, (△) $\tau = 337$, (●) $\tau = 675$.

dissipation theorem

$$\langle \eta(r,t)\, \eta(r',t') \rangle = -2Mk_B T\nabla^2\, \delta(r-r')\, \delta(t-t') \qquad (5)$$

The role of the thermal noise in domain growth and scaling has been investigated earlier, and it has been shown that the noise has no effect on the late stage growth exponent.[12,16]

For the case of symmetric polymer mixtures the free energy of the inhomogeneous system can be described using the FHD free energy functional[22] (in units of k_BT) which is given by

$$F(\phi(r)) = \int d^3r \left[f(\phi(r)) + \left(\frac{a^2}{36\phi(1-\phi)} + \chi\lambda^2 \right) |\nabla\phi(r)|^2 \right] \qquad (6)$$

where

$$f(\phi(r)) = 1/N\{\phi \ln \phi + (1-\phi) \ln (1-\phi)\} + \chi\phi(1-\phi) \qquad (7)$$

χ is the temperature-dependent Flory–Huggins interaction parameter, and a is the Kuhn length. The coefficient of the square gradient term in eq 6 has two parts: $\chi\lambda^2$ is the enthalpic part where λ is equal to the Kuhn length a and $a^2/36\phi(1-\phi)$ is the entropic part arising from the loss of conformational entropy at the interface and is evaluated within the framework of random-phase approximation.

The Onsager coefficient consistent with the Flory–Huggins theory is given by[22] $\Lambda(\phi) = ND\phi(1-\phi)$ where D is the self-diffusion coefficient of the chain. Substituting values of $\delta F(\phi(r))/\delta\phi$ and $\Lambda(\phi)$ in eq 3, we get the final equation for the evolution of the order parameter $\phi(r,t)$.

$$\frac{d\phi(r,t)}{dt} = ND\nabla\left\{\phi(1-\phi)\nabla\left[1/N \ln \frac{\phi}{1-\phi} + \chi(1-2\phi) - 2\chi a^2\nabla^2\phi - \frac{a^2}{18\phi(1-\phi)} \mathrm{del}^2{}_\phi + \frac{(1-2\phi)a^2}{36\phi^2(1-\phi)^2}(\nabla\phi)^2 \right]\right\} \qquad (8)$$

The noise term is not included in eq 8, as it only increases the number of time steps needed to obtain the asymptotic growth law. The exclusion of the noise term drastically reduces the required computer time since the repeated use of the random number generator is eliminated. Analytical studies by de Gennes[22] and later on by Binder[24] involve linearization of the above equation and hence are valid only in the early time scales of the phase separation. We compliment these studies by numerically solving the above equation which helps us to explore the kinetics of phase separation even at later time scales.

In order to facilitate comparison of the demixing behavior in various systems, the following rescaled variables are usually defined so that the experimental data can be plotted in terms of the dimensionless quantities[2,4]

$$\mathbf{x} = k_m{}^\circ\mathbf{r} \quad \text{and} \quad \tau = D_{app}(k_m{}^\circ)^2 t \qquad (9)$$

where $k_m{}^\circ$ is the wavenumber corresponding to the maximum in the structure factor at time = 0 and D_{app} is the apparent diffusivity. $k_m{}^\circ$ and D_{app} can be calculated from the linear theory. In our study, we have used the following rescaled variables:

$$\mathbf{x}_1 = \frac{(\chi-\chi_s)^{1/2}}{a}\mathbf{r} \quad \text{and} \quad \tau_1 = \frac{D(\chi-\chi_s)^2}{a^2\chi_s}t \qquad (10)$$

The values of χ at critical and spinodal points are given by $\chi_c = 2/N$ and $\chi_s = 1/(2N\phi_0(1-\phi_0))$, respectively, where ϕ_0 is the volume fraction of component A in the mixture. With these substitutions eq 8 gets rescaled as

$$\frac{d\phi(\mathbf{x}_1,\tau_1)}{d\tau_1} = \frac{1}{2\phi_0(1-\phi_0)}\nabla\left\{\phi(1-\phi)\nabla\left[\frac{\chi_c}{2(\chi-\chi_s)} \ln \frac{\phi}{1-\phi} - \frac{2\chi\phi}{\chi-\chi_s} - 2\chi\nabla^2\phi - \frac{1}{18\phi(1-\phi)}\nabla^2\phi + \frac{(1-2\phi)}{36\phi^2(1-\phi)^2}(\nabla\phi)^2\right]\right\} \qquad (11)$$

Results and Discussion

In the present study, we have taken the input parameters, viz., χ and T_c, appropriate to the symmetric system of polybutadienes primarily studied by Bates et al.[27] Thus by varying χ one can mimic the quench procedure at different final temperatures. The critical temperature (UCST) T_c is 62 °C, and the dependence of χ on temperature is given by[27]

$$\chi = 0.326/T - 0.00023 \qquad (12)$$

We have numerically integrated eq 11 on a simple cubic lattice of 32^3 with periodic boundary conditions using a time step of 0.01. The calculations reported here adopt a finite difference approximation for both the spatial and temporal derivatives. We have computed the spherically averaged structure factor $S(k,\tau)$ and the spherically averaged pair correlation function $G(x,\tau)$. Typical results of the structure factor calculation are shown in Figure 2 where $S(k,\tau)$ has been calculated in a particular run for the critical mixture quenched to 49 °C. For a given τ the scattered intensity shows a maximum for a characteristic magnitude of the wavevector, denoted by k_m and the value of k_m quantifies the most dominant length scale of the domains for that τ. We have defined a normalized correlation function $g(x,\tau) = G(x,\tau)/G(x,0)$ such that $g(x,0) = 1$. Typical results for the normalized correlation function $g(x,\tau)$ for different τ are shown in the Figure 3. Such damped oscillatory behavior of $g(x,\tau)$ has been found characteristic for the conserved order parameter systems.[11,12] The location of the first zero of the correlation function $g(x,\tau)$ is used as a quantitative measure of the domain size, $R(\tau)$. Thus the development of structure can be followed by looking at the variation of R or k_m as a function of the reduced time τ. The details of the numerical calculations are similar to those described in the ref 26.

For the critical mixture ($\phi_0 = 0.5$), we have taken the quench temperatures of 25, 35, 49, and 54.5 °C. Our

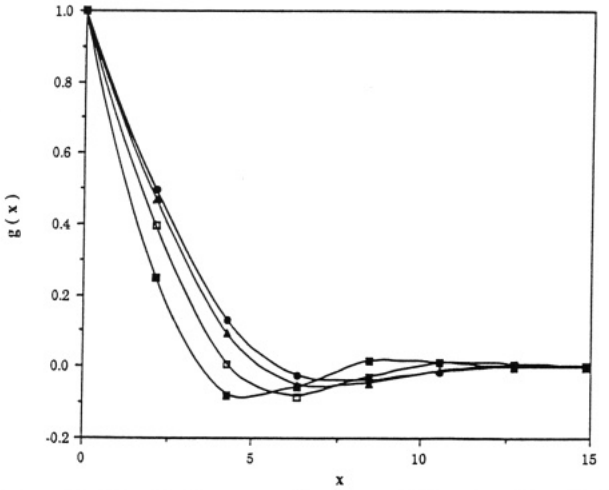

Figure 3. Spherically averaged pair correlation function $g(x,\tau)$ vs x for different values of τ calculated for the critical mixture ($\phi_0 = 0.5$) quenched to 49 °C. The symbols are as follows: (■) $\tau = 22$, (□) $\tau = 112$, (▲) $\tau = 337$, (●) $\tau = 675$.

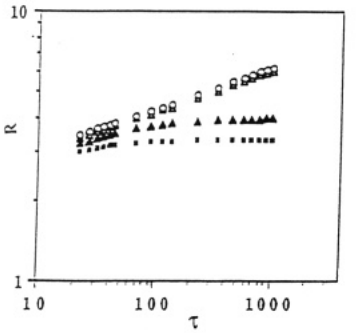

Figure 4. Time dependence of domain size R for critical ($\phi_0 = 0.5$) and off-critical ($\phi_0 = 0.4$) mixtures. The critical mixture is quenched to 54.5 (○), 49 (●), and 25 (△) °C. The off-critical mixture is quenched to 35 (■) and 15 (▲) °C.

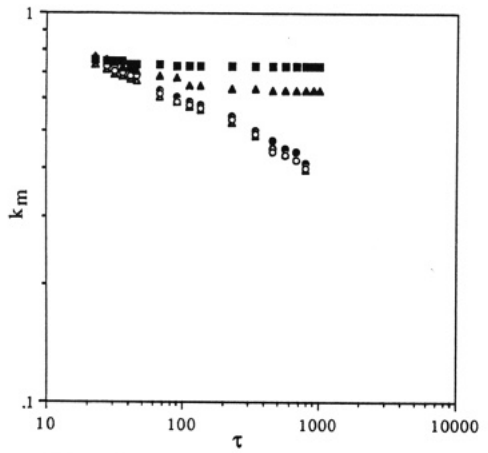

Figure 5. Time dependence of k_m for critical ($\phi_0 = 0.5$) and off-critical ($\phi_0 = 0.4$) mixtures. The critical mixture is quenched to 54.5 (○), 49 (●), and 25 (△) °C. The off-critical mixture is quenched to 35 (■) and 15 (▲) °C.

calculated results of $R(\tau)$ determined through $g(x,\tau)$ are given in Figure 4. Similarly, results for the domain size determined through k_m are plotted in Figure 5. From both of these figures it is clear that for critical mixtures the growth law does not depend on the quench temperature. The growth law exponent calculated (for $\tau > 100$) from these log–log plots is given by 0.24 (±0.02). This result is similar to the earlier study,[26] although the Onsager coefficient is now concentration dependent and the noise is left out. Our results for an off-critical mixture (ϕ_0 = 0.4) quenched to 35 and 15 °C are also shown in Figures 4 and 5. The phase-separated domains stop to coarsen after a certain characteristic time, τ_f, which is clearly seen to depend upon the quench depth, and thus the universality of the growth law is violated for the off-critical mixtures. Knowing the values of the volume fractions at every point on our 32 × 32 × 32 grid, we can generate three-dimensional images of the resulting structures at a given time during the phase separation. It is difficult to present the three-dimensional images, and, hence, the typical evolution of morphology in an arbitrary plane is presented in Figure 6. The X and Y sides of such a plane represent 32 units of the dimensionless distance which is defined in eq 10. We have used different shades of gray to represent the composition of evolving phases, where complete white corresponds to the volume fraction of the component A = 1 and complete black corresponds to the volume fraction of component A = 0. It is seen from Figure 6a that the A-rich and B-rich domains are bicontinuous at all times. In Figure 6b we see a percolated structure at $\tau_1 = 2$ for $\phi_0 = 0.4$ at 35 °C, and the pattern is similar to that of the critical quench. The contrast between the phases is weak because the phases are away from their final equilibrium compositions. However at $\tau_1 = 10$ the phases are not percolated for $\phi_0 = 0.4$ and the size of the domains is unchanged for $\tau_1 = 10$ and 200. In contrast, we see in Figure 6a that coarsening continues with τ_1 for the critical quench. Therefore, we conclude that a

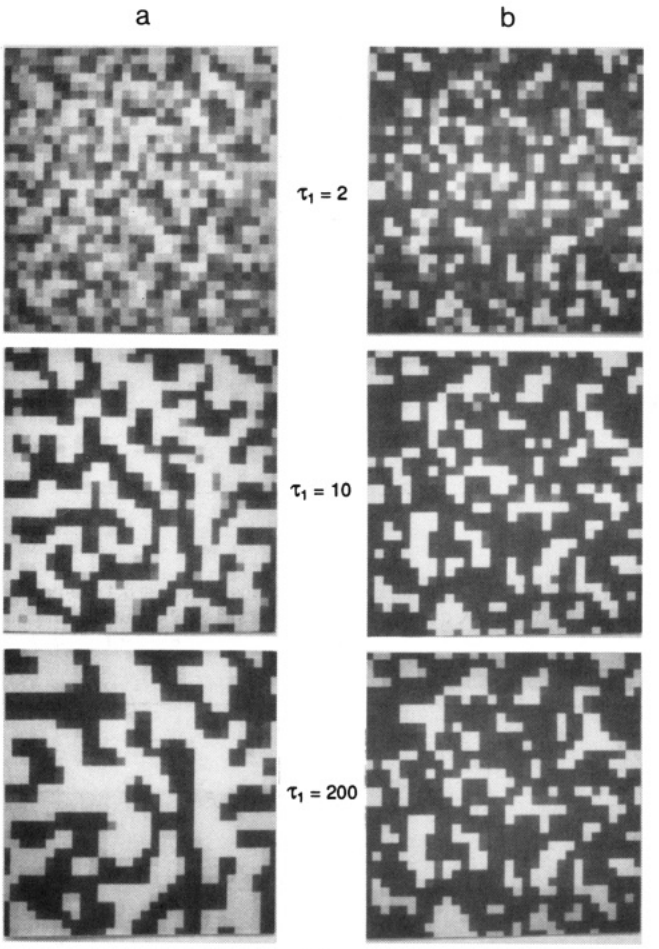

Figure 6. Computer images of the evolving phases as a function of reduced time τ_1 for (a) a critical mixture, $\phi_0 = 0.5$, and (b) an off-critical mixture, $\phi_0 = 0.4$, at 35 °C. Here the free energy functional has the entropic contribution to the gradient term. The morphology does not change for the off-critical mixture at $\tau_1 > 10$. This is to be contrasted to the growth of the percolated domains which are seen to coarsen at the same time scales.

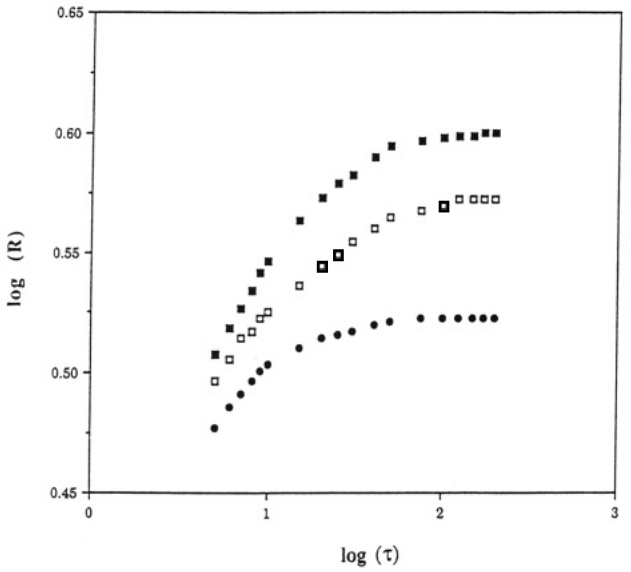

Figure 7. Off-critical mixture of composition $\phi_0 = 0.4$ quenched to three different quench temperatures; 15 (■), 30 (□), and 35 (●) °C. The sizes of the frozen domains are smaller for shallower quench depths.

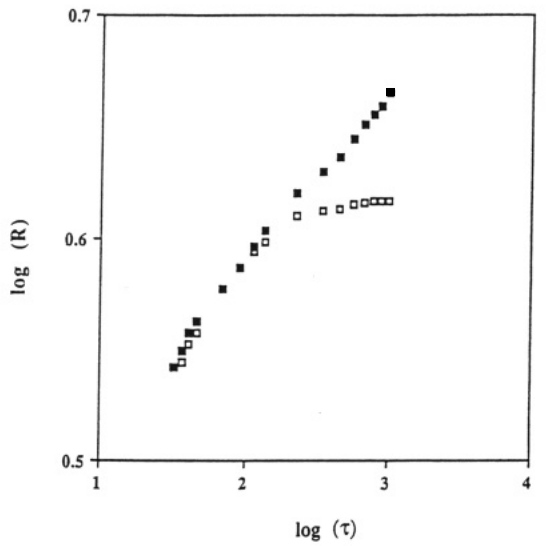

Figure 8. Domain growth arrested for the off-critical mixture of composition $\phi_0 = 0.45$ when quenched to 50 °C (□). The same composition shows unarrested coarsening of domains when quenched to 46 °C (■).

morphological pattern is frozen for $\phi_0 = 0.4$ at 35 °C even though this condition belongs to the SD regime.

The effect of quench depth on the growth of domains in the case of off-critical mixtures is illustrated by the $R(\tau)$ data for $\phi_0 = 0.4$ and $\phi_0 = 0.45$ plotted in Figures 7 and 8, respectively. As seen from Figure 7 we find that for $\phi_0 = 0.4$ freezing occurs at all three quench temperatures (15, 30, and 35 °C) studied here. It is also clear that the freezing occurs earlier at shallower quench depths and the corresponding domain sizes are smaller. From Figure 8 we see that the domain growth is not arrested for $\phi_0 = 0.45$ quenched to $T = 46$ °C but the domain growth is arrested when quenched to 50 °C. For these cases, the typical morphology in an arbitrary plane at time $\tau_1 = 250$ is shown in Figure 9. In Figure 9a the domains of the minority phase are dispersed in the majority phase and the coarsening is stopped as is seen from Figure 8. While in Figure 9b it is seen that the two phases are highly interconnected and the coarsening of domains is not arrested in this case. Thus when the mixture of initial

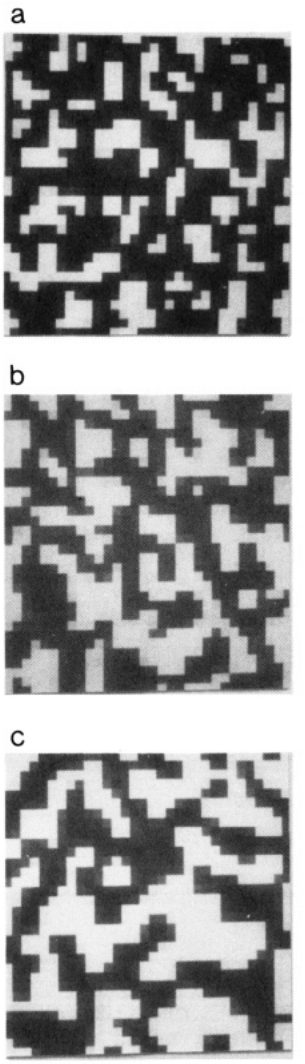

Figure 9. Images of the evolved domains at $\tau_1 = 250$ shown for the off-critical composition $\phi_0 = 0.45$ quenched to 50 (a), 46 (b), and 25 °C (c). Dispersed domains are formed in a while interconnected domains are formed in b and c.

composition $\phi_0 = 0.45$ is quenched to 46 °C, the volume fraction of the minority phase is sufficiently high so as to form interconnected domains and these domains coarsen, unlike the dispersed domains which are formed when the same mixture is quenched to 50 °C. From parts a–c of Figure 9 it is seen that the volume fraction of the minority phase is higher for deeper quench depths and so is the interconnectivity of the domains.

The relative volume fractions of the equilibrium phases for a given ϕ_0 and T are obtained from the lever rule. If the volume fraction of the minority phase is less than the percolation threshold, the structure has dispersed domains of the minority phase in the matrix of the majority phase. If the dispersed domains can be formed, then they may not grow due to the entropic barriers for chain transport across sharp interfaces. Thus, for a given phase diagram there is a region inside the unstable region where the two equilibrium phases can be percolated and is associated with the unarrested coarsening of the domains. There is also a region where the domains of the minority phase will have dispersed clusters and is associated with the arrested coarsening of the phase-separated domains. The boundary of this region of frozen morphology inside the unstable region is obtained by repeating the above calculations for different values of ϕ_0 and T. For the system studied here this region is given in Figure 10 along with the binodal and

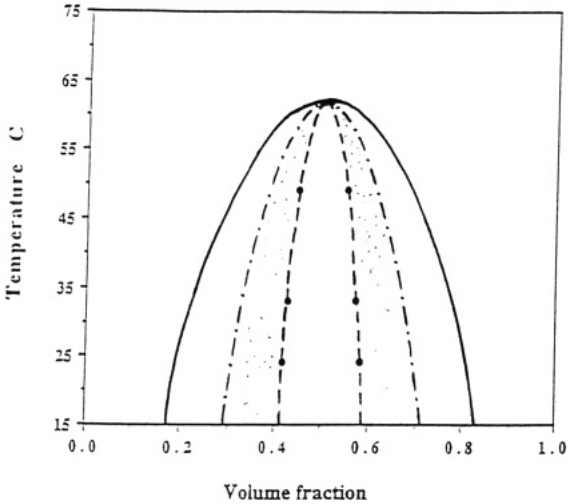

Figure 10. Calculated binodal (—) and spinodal curves (- • -) for the particular polymer blend in this study. The dotted line (- - -) represents the transition from the percolated to the dispersed morphology based on the percolation threshold of 0.37. This percolation threshold is calculated based on the data points (shown in dark circles on this line) where the growth of the domains was no longer arrested. The shaded region between the spinodal curve and the dispersed to percolated clusters transition line depicts the transnodal region.

spinodal curves. We call this new region of frozen morphology the "transnodal region".[28]

While the transition from percolated to dispersed clusters occurs for all off-critical systems, whether small or large molecules, the freezing of the patterns is triggered only for the polymer case due to the above-discussed entropic barriers for chain transport across the interfaces. (Note that the significance of "off-criticality" in the present context is closely related to the symmetry of the phase diagram.) This can be directly verified by suppressing the entropic contribution to the interfacial free energy in eq 6 and repeating the calculations. In this spirit we also performed calculations starting with the free energy functional

$$F(\phi(r)) = \int d^3r\, [f(\phi(r)) + \kappa|\nabla\phi(r)|^2] \qquad (13)$$

where $f(\phi)$ is the Flory–Huggins free energy and $\kappa|\nabla\phi|^2$ is the enthalpic contribution to the free energy density from the local composition gradients. Now the reduced variables are defined as

$$\mathbf{x} = \frac{(\chi - \chi_s)^{1/2}}{\chi^{1/2}\lambda}\mathbf{r} \quad \text{and} \quad \tau = \frac{D(\chi - \chi_s)^2}{\chi\lambda^2\chi_s}t \qquad (14)$$

After rescaling the corresponding differential equation with the above variables and solving the resulting differential equation in the same previously mentioned manner, we have plotted our results of the domain size, $R(\tau)$, for $\phi_0 = 0.4$ and $T = 35$ and 40 °C in Figure 11. Clearly the free energy functional of eq 13 does not show freezing of the morphology for the off-critical mixtures at the same quench temperatures as before. A typical evolution of morphology in an arbitrary plane is shown in Figure 12. In sharp contrast to Figure 6b, Figure 12 reveals that the droplets of the dispersed phase grow without any freezing as in small-molecule systems where larger droplets cannibalize smaller droplets. The only difference between Figures 6b and 12 is the entropic contribution to the interfacial free energy. The free energy functional of eq 13 is similar to the small-molecule case in terms of a composition-independent prefractor of the gradient term

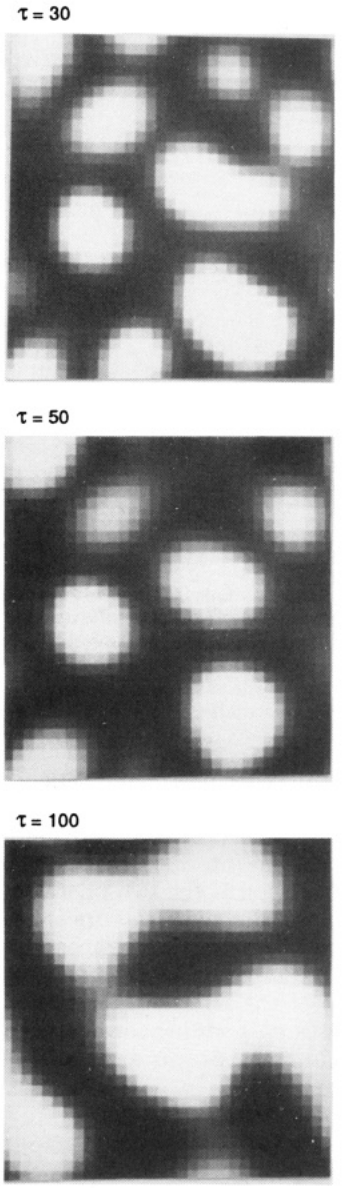

Figure 11. Time dependence of domain size R for the off-critical ($\phi_0 = 0.4$) mixture quenched to 35 (●) and 40 (○) °C. Here the free energy functional has only the enthalpic contribution to the gradient term.

and only differs in the homogeneous free energy, which in the case of polymers is given by the Flory–Huggins free energy. The results obtained with the free energy functional of eq 13 are not surprising in view of the known experimental and numerical results in the phase separation of off-critical mixtures of small-molecule systems.[14-16] In eq 13 λ is the effective interaction length between polymer molecules. In the FHD free energy functional λ is taken equal to the Kuhn length, a, and hence for small values of χ, as for the polymer blend in this study, the FHD free energy functional has dominance of the entropic contribution to the interfacial free energy. However, if λ is on the order of the radius of gyration of the chain, then it is possible to realize a significant enthalpic contribution to the interfacial free energy. In fact Debye[24] has obtained the value of λ equal to $R_g/6$ for inhomogeneous polymer solutions where R_g is the radius of gyration of the polymer chain.

Lifshitz and Slyozov[17] and later on Voorhees and Glicksman[29] analyzed the growth of dispersed domains and found that the asymptotic growth law is of the form $R(t) \sim t^{1/3}$. In both of these analyses the volume fraction of the

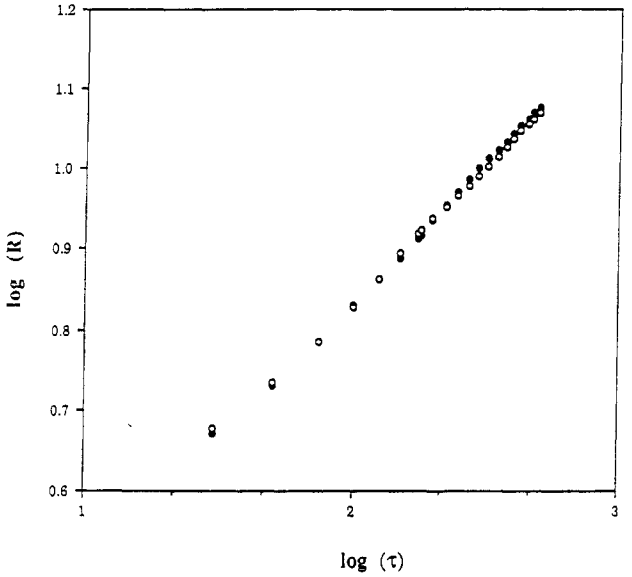

Figure 12. Computer images of the evolving phases as a function of reduced time τ for an off-critical mixture ($\phi_0 = 0.4$) quenched to 35 °C. Here the free energy functional has only the enthalpic contribution to the gradient term similar to the small-molecule case. The growth of the dispersed domains is seen to occur by the classical mechanism where larger domains grow at the expense of smaller domains. τ is defined in eq 13.

minority phase is considered small enough so as to form isolated domains in the matrix of the majority phase and the coarsening occurs by the transport of molecules perpendicular to the interface. Huse[18] argued that when the volume fractions of the two phases are comparable, then the resulting domain structure is highly percolated and there exists another mode of transport which is parallel to the interface in addition to the transport occurring perpendicular to the interface. He generalized the Lifshitz–Slyozov law by adding corrections on the of order $1/R(t)$ to account for the transport parallel to the interface as

$$\frac{dR(t)}{dt} = \frac{C_2}{R^2(t)} + \frac{C_3}{R^3(t)} + O(R^{-4}) \qquad (15)$$

where C_3 and C_2 are numerical coefficients. For dispersed domains $C_3 = 0$ and $C_2 > 0$ and we obtain the Lifshitz–Slyozov growth law $R(t) \sim t^{1/3}$. For percolated domains, $C_3 > 0$ and we obtain at large R and t

$$R(t) = (C_3/2C_2) + (3C_2t)^{1/3} \qquad (16)$$

If the chain transport perpendicular to the interface is totally absent, then $C_2 = 0$ and $C_3 > 0$ and one obtains the growth law $R(t) \sim t^{1/4}$. Kawasaki and Sekimoto[30] have also obtained a similar growth law by considering the transport parallel to the interface as the mechanism of coarsening. Our results of the calculations for the critical mixtures using the FHD functional can be fitted to the growth law of the form $R(t) \sim t^n$ as in Figure 4 with the exponent $n = 0.24$ (±0.02), which is close to the "quarter" power law described before. $R(\tau)$ data for the critical mixture quenched to 54.5 °C are plotted as a function of $\tau^{1/3}$ in Figure 13. These data can be fitted to the generalized growth law in eq 16 with $C_2 = 0.018$ and $C_3 = 0.094$ suggesting that the coarsening is dominated by the transport parallel to the interface. We can also fit the data to the generalized power law of the type $R(t) = A_2 + B_2t^{1/4}$ as shown in Figure 14. Although the quarter power law fit is slightly better than the one-third power law fit, we cannot conclusively say that the growth is described by any particular form of the growth law. The magnitude

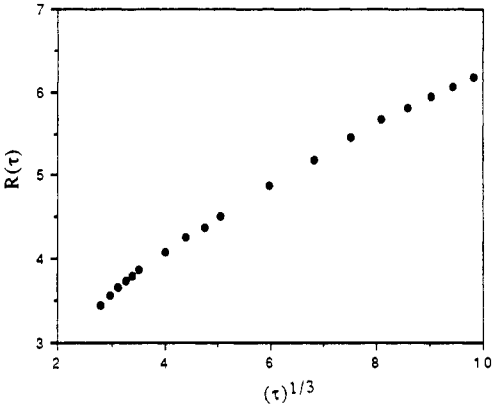

Figure 13. $R(\tau)$ data for the critical mixture quenched to 54.5 °C plotted as a function of $\tau^{1/3}$.

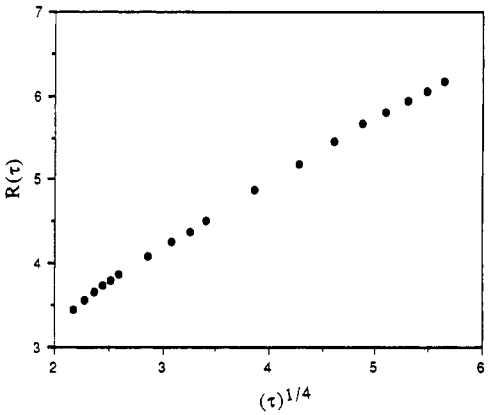

Figure 14. $R(\tau)$ data for the critical mixture quenched to 54.5 °C plotted as a function of $\tau^{1/4}$.

of the entropic barriers in our mechanism depends on the concentration difference between the phase-separated domains (i.e., how steep the composition gradient is in the interface). In the early stages of the SD process when the interfaces are not sharp the coarsening can occur by both the parallel and perpendicular modes of transport. However in the later stages, when the interfaces are sharper, only the transport parallel to the interface dominates. On the other hand, our results of the calculations for the off-critical mixture ($\phi_0 = 0.4$) using the free energy functional of eq 13 can be fitted to the growth law of the type $R(t) \sim t^n$ with the exponent $n = 0.32$ (±0.02), which is very close to the Lifshitz–Slyozov predictions. This free energy functional has no entropic contribution to the interfacial free energy and shows the unarrested coarsening of the isolated domains by the classical Lifshitz–Slyozov type evaporation–condensation mechanism.

We have also analyzed our data to test the validity of the dynamical scaling at late time scales during the SD process. The scaling hypothesis states that there exists only one length scale dominating the dynamics in the scaling regime and the topology scales with time. This dominant length scale is the characteristic size of the domains, $R(\tau)$. According to the dynamical scaling ansatz, there exists a time-independent function $F(k,R(\tau))$ such that $I(k,\tau) = R(\tau)^d F(k,R(\tau))$ where $I(k,\tau)$ is the scattered light intensity and d is the space dimensionality. We have tested the dynamical scaling law by plotting $I(k,\tau)$ $k_m(\tau)^3$ as a function of k/k_m as shown in parts a–d of Figure 15 for various compositions and quench temperatures and by checking if the function $F(k/k_m)$ is independent of time. In each of the cases we get a time-independent scaling function $F(k/k_m)$, and thus we observe the validity of the dynamical scaling law at late time scales in the SD process.

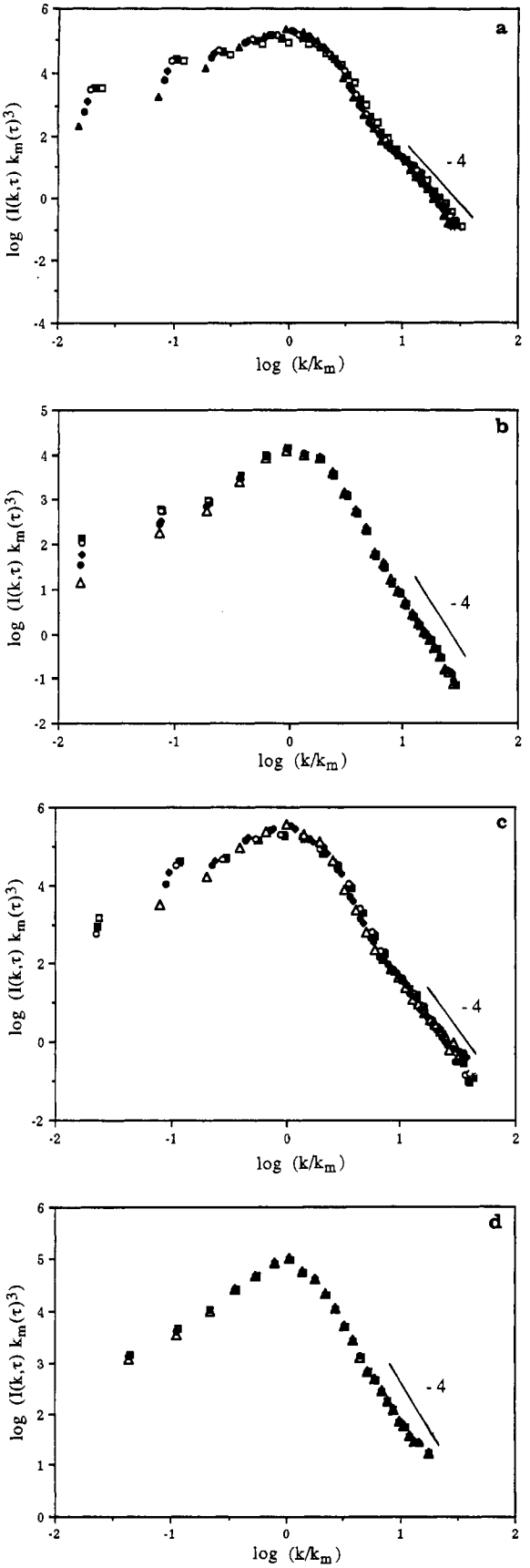

Figure 15. $I(k,\tau)\ k_m(\tau)^3$ is plotted as a function of (k/k_m) on a log–log scale for the following cases: (a) $\phi_0 = 0.5$ and $T = 35$ °C; (b) $\phi_0 = 0.45$ and $T = 50$ °C; (c) $\phi_0 = 0.45$ and $T = 25$ °C; (d) $\phi_0 = 0.4$ and $T = 35$ °C. The symbols are as follows: (▲) $\tau = 225$, (●) $\tau = 337$, (◆) $\tau = 450$, (○) $\tau = 675$, (■) $\tau = 787$, (□) $\tau = 900$. The solid line shows the k^{-4} behavior.

Figure 15a shows the functional form of $F(k/k_m)$ for a critical mixture $\phi_0 = 0.5$ quenched to 35 °C. The scaling function shows a weak shoulder, and it follows a $k^{-3.6}$ power law for large k. The presence of a weak shoulder has been observed in the recent experimental and simulation studies.[2,4,26] Similar behavior is observed for the critical mixture quenched to 49 and 25 °C. We have constructed similar plots for the off-critical mixture $\phi_0 = 0.45$ quenched to 50 and 25 °C in parts b and c of Figure 15, respectively. We know that the off-critical mixture $\phi_0 = 0.45$ quenched to 50 °C shows freezing of the morphology, and in this case we observe that the scaling function does not show a shoulder and follows a k^{-4} power law for large k as seen from Figure 15b. This is to be contrasted with the form of the scaling function shown in Figure 15c. In this case ($\phi_0 = 0.45$ and $T = 25$ °C) we have found above that the system has highly interconnected domains of the two coexisting phases and shows unarrested coarsening of the phase-separated domains. Here we see the emergence of the shoulder, and the scaling function follows a $k^{-3.6}$ power law for large k. In Figure 15d we have plotted the data for the off-critical mixture $\phi_0 = 0.4$ quenched to 35 °C which shows freezing of the morphology and we see behavior similar to that of Figure 15b.

The observation of the scaling behavior, $F(x) \sim x^{-4}$ (where $x = k/k_m$), for large k in these numerical calculations is in agreement with the expected Porod's law for large k values. This law should appear whether the system's morphology is frozen or not, as observed in the present calculations. However, if the composition and temperature are such that the system is not in the transnodal regime, then the $F(x) \sim x^{-6}$ behavior characteristic of percolated structures[32] is expected for $1 < x \leq 2$. The crossover from the approximately x^{-6} behavior for $1 < x \leq 2$ to x^{-4} behavior for $x > 2$ is seen in parts a and c of Figure 15. On the other hand, x^{-6} behavior should be absent in the transnodal regime as observed in parts b and d of Figure 15. These observations offer further support to the phase diagram presented in Figure 10 and the proposed mechanism for the formation of frozen morphologies.

Conclusions

The major conclusions of the present study may be summarized as follows:

(1) We have found a novel regime for off-critical mixtures of symmetric polymer blends where growth is suppressed although the system is thermodynamically unstable. This regime, called the transnodal regime, appears between the spinodal line and a region around the critical composition. We have shown that this regime originates from the formation of clusters of the minority phase and the entropic barrier associated with the transport of long chains across sharp interfaces. We have also shown that the percolated structure formed in the early stage of the SD process can undergo percolated to dispersed domain transitions depending upon the relative volume fractions of the two coexisting phases, which are decided by the lever rule of the phase diagram. This enables us to identify the boundaries of the transnodal region. The arrest of the coarsening of the phase-separated domains is not observed in the case of off-critical mixtures of small-molecule systems. It is therefore necessary to perform experiments on model blends to distinguish between the proposed mechanism and the high viscosity effect postulated in a preliminary observation[32] of pinned structures.

(2) The growth law obtained for the critical mixtures is independent of the quenched depth, and if fitted to the power law of the type $R(t) \sim t^n$, we obtain $n = 0.24$ (±0.02) which is close to the quarter power law predicted for the coarsening of domains dominated by the molecular trans-

port parallel to the interface. The same data can also be fitted to the generalized Lifshitz–Slyozov law of the type $R(t) = A + Bt^{1/3}$.

(3) We observe the validity of the dynamical scaling laws for the critical and off-critical mixtures at late time scales during the SD process. We show that the tail of the scaling function exhibits k^{-4} behavior (Porod's law) for both the critical and off-critical mixtures. However, there is a shoulder arising from the crossover from k^{-6} behavior to the k^{-4} behavior in the case of percolated morphologies.

Acknowledgment. We thank Dr. A. Chakrabarti for discussions and his generous help in the numerical part of this work. We also thank K. G. Koniaris for his help in making the images. We are grateful to Dr. E. A. Di Marzio for suggesting the name transnodal. This work was supported by NSF Grant DMR-90081900 and the Materials Research Laboratory at the University of Massachusetts at Amherst.

References and Notes

(1) Schwahn, D.; Mortensen, K.; Yee-Madeira, H. *Phys. Rev. Lett.* **1987**, *58*, 1544.
(2) Wiltzius, P.; Bates, F. S.; Heffner, W. R. *Phys. Rev. Lett.* **1988**, *60*, 1538.
(3) Bates, F. S.; Rosedale, J. H.; Stepanek, P.; Lodge, T. P.; Wiltzius, P.; Fredrickson, G. H.; Hjelm, R. P., Jr. *Phys. Rev. Lett.* **1990**, *65*, 1893.
(4) Hashimoto, T.; Itakura, M.; Hasegawa, H. *J. Chem. Phys.* **1986**, *85*, 6118. Hashimoto, T.; Itakura, M.; Shimidzu, N. *J. Chem. Phys.* **1986**, *85*, 6773. Hashimoto, T. *Phase Transitions* **1988**, *12*, 47.
(5) For a review, see: Gunton, J. D.; San Miguel, M.; Sahni, P. S. In *Phase Transitions and Critical Phenomena*; Domb, C., Lebowitz, J. L., Eds.; Academic Press: New York, 1983; Vol. 8.
(6) Klein, J. *Science* **1990**, *250*, 640.
(7) Helfand, E.; Tagami, Y. *J. Chem. Phys.* **1971**, *56*, 3592. Helfand, E.; Sapse, A. M. *J. Chem. Phys.* **1975**, *62*, 1327. Helfand, E. *Macromolecules* **1976**, *9*, 307.
(8) Szleifer, I.; Widom, B. *J. Chem. Phys.* **1989**, *90*, 7524.
(9) de Gennes, P.-G. *Scaling Concepts in Polymer Physics*; Cornell University: Ithaca, NY, 1979.
(10) Cahn, J. W.; Hilliard, J. E. *J. Chem. Phys.* **1958**, *28*, 258. Cook, H. E. *Acta. Metall.* **1970**, *18*, 297.
(11) Toral, R.; Chakrabarti, A.; Gunton, J. D. *Phys. Rev. Lett.* **1988**, *60*, 2311. Chakrabarti, A.; Toral, R.; Gunton, J. D. *Phys. Rev. B* **1989**, *39*, 4386.
(12) Rogers, T. M.; Elder, K. R.; Desai, R. C. *Phys. Rev. B* **1988**, *37*, 9638. Puri, S.; Oono, Y. *J. Phys. A* **1988**, *21* (15), L755.
(13) Amar, J. G.; Sullivan, F. E.; Mountain, R. D. *Phys. Rev. B* **1988**, *37*, 196.
(14) Labowitz, J. L.; Marro, J.; Kalos, M. H. *Acta. Metall.* **1982**, *30*, 297.
(15) Oono, Y.; Puri, S. *Phys. Rev. Lett.* **1987**, *58*, 836. Puri, S.; Oono, Y. *Phys. Rev. A* **1988**, *38*, 1542.
(16) Toral, R.; Chakrabarti, A.; Gunton, J. D. *Phys. Rev. B* **1989**, *39*, 901.
(17) Lifshitz, I. M.; Slyozov, V. V. *J. Phys. Chem., Solids* **1961**, *19*, 35. Langer, J. S. *Ann. Phys.* **1971**, *65*, 53. Binder, K.; Stauffer, D. *Phys. Rev. Lett.* **1974**, *33*, 1006. Siggia, J. S. *Phys. Rev. A* **1979**, *20*, 595. Ohta, T. *Ann. Phys. (New York)* **1984**, 158.
(18) Huse, D. A. *Phys. Rev. B* **1986**, *34*, 7845.
(19) Nishi, T.; Wang, T. T.; Kwei, T. *Macromolecules* **1975**, *8*, 227.
(20) Mcmaster, L. P. In *Copolymers, Polyblends and Composites*; Platzer, N. A., Ed.; Advances in Chemistry Series 142; American Chemical Society: Washington, DC, 1975; p 43.
(21) Debye, P. *J. Chem. Phys.* **1959**, *31*, 680.
(22) de Gennes, P.-G. *J. Chem. Phys.* **1980**, *72*, 4756.
(23) Tang, H.; Freed, K. F. *J. Chem. Phys.* **1991**, *94*, 1572.
(24) Pincus, P. *J. Chem. Phys.* **1981**, *75*, 1996. Binder, K. *J. Chem. Phys.* **1983**, *79*, 6387.
(25) Sariban, A.; Binder, K. *Macromolecules* **1991**, *24*, 578.
(26) Chakrabarti, A.; Toral, R.; Gunton, J.; Muthukumar, M. *J. Chem. Phys.* **1990**, *92*, 6899.
(27) Bates, F. S.; Wignall, G. D.; Koehler, W. C. *Phys. Rev. Lett.* **1985**, *55*, 2425.
(28) Di Marzio, E. A., suggested the name transnodal.
(29) Voorhees, P. W.; Glicksman, M. E. *Acta Metall.* **1984**, *32*, 2001.
(30) Kawasaki, K.; Sekimoto, K. *Macromolecules* **1989**, *22*, 3063.
(31) Furukawa, H. *Physica* **1984**, *A123*, 497; *Phys. Rev.* **1986**, *B33*, 638.
(32) Hashimoto, T. In *Dynamics of Ordering Processes in Condensed Matter*; Komura, S., Ed.; Plenum Press: New York, 1988.